Electron–phonon coupling in lightly *n*-doped 1T monolayers of PdSTe and PdSeTe: A rigid band approximation approach

Elie A. Moujaes [a], W.A. Diery [b],*

[a] *Physics Department, Federal University of Rondônia, 76900-900, Porto Velho, Brazil*
[b] *Physics Department, Faculty of Science, King AbdulAziz University, 21589, Jedda, Saudi Arabia*

A B S T R A C T

In this paper, we present a preliminary study to determine the electron–phonon (el–ph) coupling in Janus 1T monolayered PdSTe and PdSeTe within the rigid band approximation (RBA). Under the assumption that both electronic band structures and phonon dispersions remain intact, or suffer slight changes at most, the Fermi energy is manually shifted towards the conduction bands. Without spin–orbit coupling (SOC), these structures are predicted to be semiconductors with electronic bandgaps of 0.33 eV for PdSTe and 0.34 eV for PdSeTe and with an insignificant electron–phonon coupling. We find that minimal small Fermi energy shifts of the order of 35 meV and 65 meV applied to 1T PdSTe and PdSeTe respectively, are sufficient to produce non-zero values of λ in both systems. These shifts could physically correspond to small electron doping of the materials, not exceeding 4%. Our calculations give that $\lambda = 1.77$ and $\lambda = 0.5$ for PdSTe and PdSeTe respectively. The corresponding lowest superconducting temperatures (T_c) register 0.28 K for PdSeTe and 28.19 K for PdSTe. We also demonstrate that the longitudinal optical and acoustical phonon modes may play a key role in the process of superconductivity of the doped materials. The above temperature of PdSTe is larger than those for 2D borophene, stanene, phosophorene and arsenene indicating that, in principle if the right dopant is found, lightly *n*-doped PdSTe could be promising in the area of 2D superconductors.

1. Introduction

Two-dimensional materials (2D) are crystalline structures made up of one single layer of atoms. Almost 78 years ago, such materials were not supposed to exist [1,2] and thus were deemed thermodynamically unstable. The synthesis of graphene [3], a 2D sheet of carbon, one-atomic layer thick, took the world by surprise. This material is special in a variety of ways: other than being a null gap semiconductor, with linear and isotropic bands around the K point in the reciprocal hexagonal Brillouin zone [4], it is very malleable and absorbs almost 2.3% of the incident light; this makes it useful in light crystal liquids (LCD) applications such as touchscreen displays [5] and in solar cells [6]. Graphene has also a high optical conductivity [7] and is almost 200 times stronger than steel [8].

Graphene's tremendous properties set forth the possibility for other types of 2D systems to exist with equally or even better characteristics. Such 'post graphene' materials include silicene [9], germanene [10], phosphorene [11], borophene [12], arsenene [13], diamondene [14], and plumbene [15] -which was recently synthesized [16]- amongst others.

New types of 2D structures, called transition metal dichalcogenides (TMD) have also caught attention and have been (and are still being) researched by scientists. They are represented by the chemical formula MX_2, where M is a transition metal and X = S, Se or Te. The first structures to be studied were monolayers of MoX_2 and WX_2 showing indirect band gaps as opposed to direct band gaps that emerge in their bulk structures [17]. Electronic band structure and stability were later inspected in other TMDs with M = Ti, Zr, Hf, V, Nb, Ta and Cr [18–22].

Derived from the TMDs and by substituting one layer of X = S, Se and Te by a layer of another element Y of the same set {S, Se, Te}, Janus TMD structures (called MXY structures) can be formed. Few achievements on both a theoretical and experimental level have been made: MoSSe layers were synthesized using different techniques [23]. The stability and thermoelectric properties of ZrSSe [24] and monolayer and bilayer MoSSe [25] have been reported. Also recently we have examined the thermoelectric properties and the figure of merit (ZT) for the Pd pristine and Janus structures namely PdS_2, $PdSe_2$, PdSSe, PdSTe and PdSeTe [26].

Another enticing property in materials is superconductivity, which is the phenomenon of conducting electricity with zero resistance.

Already established superconductors range from Hg and Pb, ceramics (MgB$_2$ [27], YBCO [28]) up to pnictides such as fluorine-doped LaOFeAs [29]. One practical use of a superconductor is to construct powerful electromagnets to accelerate particles very fast (such as the ones used in the Large Hadron Collider (LHC)); they can also be found in Superconducting Quantum Interference Devices (SQUID) [30] that, other than detecting weak magnetic fields, are used as a part of the equipment utilized in the removal of land mines. Generating electricity in more efficient ways as well as fast computing are other goals of superconductors that nowadays are still under development. Since the well known classical superconductors have low values of T_c [31], there has been a lot of attempts to find systems where the superconducting state is characterized by higher T_c values. Very recently a group of researchers have claimed to reach an almost room temperature superconductivity of ~285 K for a compound made from sulfur, hydrogen and carbon, under conditions of extreme pressure [32].

Graphene, for example, is not a superconductor. However intercalating monolayer graphene with Ca [33] or twisting two graphene layers by a "magic" angle [34] seem to awaken superconductivity. [35] reported evidence of superconductivity in bilayer graphene intercalated with Ca but not with Li, demonstrating the importance of the intercalated atomic species. Recent findings have also shown that bilayer graphene intercalated with alkali and alkaline earth metals namely K, Sr and Rb is superconducting with T_c values within the range 5.47–14.56 K. [36].

2D superconductors, in particular, are important because of the quantum phenomena they provide. This area of research has been active over the last 83 years [37] and started gaining fame after 1980. At the time, the concept of thin film superconductors [38–41] have started to emerge. The fabrication of monolayer cuprate superconductors took place in the early 1990s [42,43]. Since then, some new fabrication techniques have begun to erupt such as molecular beam epitaxy (MBE); also mechanical exfoliation and field effect devices have been considered amongst researchers in the area of 2D superconductors [44–47].

On a theoretical level, some studies have been performed to look into superconductivity in 2D crystals, other than graphene, by calculating the electron–phonon (el–ph) coupling coefficient (λ). This was done for some structures of graphyne [48,49], an allotrope of carbon where triple carbon bonds are introduced into the honeycomb lattice; the scattering mechanism in such structures [50] is shown to be driven by the longitudinal acoustic (LA) mode. The el–ph interactions have also been examined in borophene [51], silicene, germanene [52], electron-doped arsenene [53] and in 2D Mo$_2$B$_2$ [54].

As far as TMDs are concerned, there are a few papers dedicated to the study of the el–ph interactions: [55] discusses the el–ph interactions for an MoS$_2$ monolayer where a Debye model is used to obtain the el–ph coupling parameter. Superconductivity in both bulk and monolayer TaS$_2$ structures was investigated in [56] showing that there is no phonon mediated enhancement of T_c in the monolayer compared to the bulk. The competition between Coulomb and el–ph interactions in 2D NbS$_2$ systems is discussed in [57]. Also the superconducting order in 2H TaSe$_{2-x}$S$_x$ has been thoroughly examined in [58]. However not a lot has been done on el–ph interactions in Janus structures: Only very recently, enhanced el–ph scattering in Janus MoSSe structures has been reviewed [59].

In this paper, we investigate the response of the el–ph coupling in 2D 1T PdSTe and PdSeTe, to the manual shifting of the Fermi energy (E_{F0})) towards the conduction bands, in an attempt to mimic small electron doping (n-doping). Since both the band structure and the phonon dispersion curves, which will be reproduced using maximally localized Wannier functions (MLWFs), are supposed to stay unaltered during the doping process, the el–ph coupling as well as the superconducting temperatures (T_c), can be studied within a rigid band approximation scheme [60]. The paper is organized as follows: In Section 2, the computational method using MLWFs [61] and the Migdal–Eliashberg theory to calculate the el–ph interaction are presented. Convergence

with respect to certain parameters is checked in Section 3. The results obtained, followed by a discussion, are the main subject of Section 4. Finally, Section 5 contains a summary of the main conclusions of this work.

2. Computational methods and the Migdal–Eliashberg theory

As a first step, a self-consistent first-principles calculation was run using the plane wave Quantum Espresso (QE) package [62]. To model the interaction between the valence electrons and the ion cores, a norm-conserving (NC) Troullier–Martins pseudopotential [63] with a scalar relativistic Perdew–Burke–Ernzerhof (PBE) parametrization was used to account for the exchange correlation function [64]. A dense electronic **k**-points grid of $24 \times 24 \times 1$, in the reciprocal Brillouin zone (BZ), was adopted to ensure convergence for the electronic as well as the subsequent phonon calculations. A plane wave energy cutoff of 75Ry was utilized together with a tight geometry relaxation until the force acting on each atom in the unit cell is 5×10^{-4} Ry/au and the pressure is less than 0.16 kbar. Finally in order to model a 2D structure, a vacuum distance of 18 Å was added along the non-periodic direction, perpendicular to the plane of the systems. It is also important to note that the subsequent calculations do not take the SOC into account.

Phonon dispersion calculations are carried out within QE, where a convergent phonon **q**-grid of $12 \times 12 \times 1$ is adopted. Since the Fermi energy is rigidly shifted, we resort to the EPW (Electron–Phonon-Wannier) package [65,66] to determine the el–ph coefficient λ. EPW employs MLWFs to generate accurate el–ph matrix elements on arbitrary dense Brillouin zone grids using a Fourier interpolation technique. Both electronic and phonon band structures are reproduced from the MLWFs making use of the WANNIER90 package [67]. Fourteen Wannier functions were employed to model nine valence and five conduction bands for the systems at hand. Within EPW, coarse electronic and phonon meshes, on which the perturbation potentials [65] are evaluated, are chosen to be $48 \times 48 \times 1$ and $12 \times 12 \times 1$ respectively. Fine **k** and **q** grids of $240 \times 240 \times 1$ are then used to interpolate the el–ph coupling quantities and produce convergent results. It is equally important to correctly tune the parameter which refers to smearing in the energy-conserving delta functions. The values of this parameter must preferably lie between 1 and 10 meV. We have set this variable to 5 meV and verified that our values converge for the fine grids quoted above.

The computation of the el–ph coupling parameter λ is based on solving the isotropic Migdal–Eliashberg equations [68]. Unlike the Bardeen–Cooper–Shrieffer (BCS) [69] theory, superconductors within the Eliashberg theory, are described by taking into account the retarded nature of the electron–boson interaction that mediates the Cooper pairing [70,71]. The isotropic Eliashberg spectral function reads:

$$\alpha^2 F(\omega) = \frac{1}{2\pi N(E_F)} \sum_{q\nu} \delta(\omega - \omega_{q\nu}) \frac{\gamma_{q\nu}}{\hbar \omega_{q\nu}}, \tag{1}$$

where $\gamma_{q\nu}$ and $\omega_{q\nu}$ are the linewidth and frequency of mode ν at the phonon wavevector **q** respectively and $N(E_F)$ is the density of states (DOS) at the Fermi level.

The el–ph coupling parameter $\lambda_{q\nu}$, for the state (**q**, ν) is given by:

$$\lambda_{q\nu} = \frac{\gamma_{q\nu}}{\pi \hbar N(E_F) \omega_{q\nu}^2}. \tag{2}$$

The net el–ph coupling parameter is the sum over all possible states (**q**, ν), defined as:

$$\lambda = \sum_{q,\nu} \lambda_{q\nu} = 2 \int \frac{\alpha^2 F(\omega)}{\omega} d\omega, \tag{3}$$

where the integration extends over the entire phonon spectrum. Once λ is calculated, a superconducting transition temperature T_c can be obtained, making use of the McMillan–Allen–Dynes expression [72,73]:

$$T_c = \frac{\omega_{log}}{1.2} exp\left[\frac{-1.04(1+\lambda)}{\lambda(1 - 0.62\mu^*) - \mu^*}\right]; \tag{4}$$
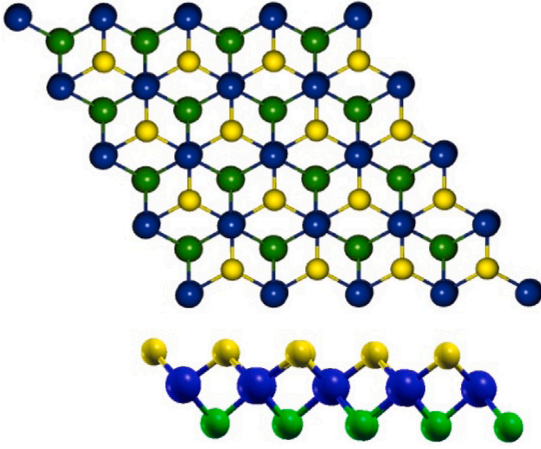
Fig. 1. (Color online). Top and side views of a (4 × 4) unit cell of the 1T Janus Pd dichalcogenides. Blue spheres are Pd atoms; yellow spheres refer to either S or Se whereas Te atoms are represented by green spheres.
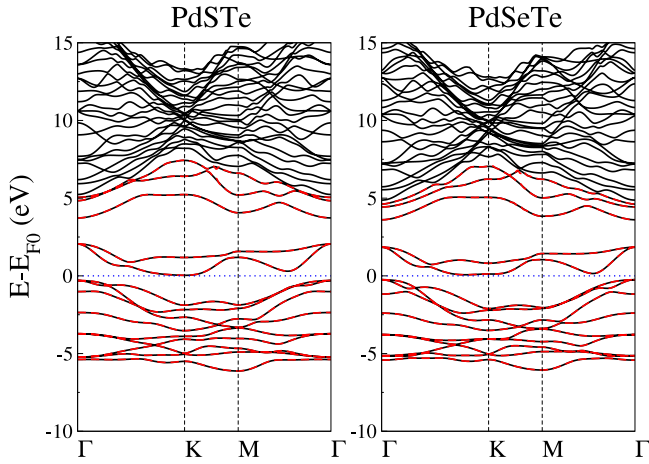
Fig. 2. (Color online). Electronic bands obtained via Density Function Theory (DFT) (solid black curves) using QE [26] and those reproduced using MLWFs (dashed red curves), for PdSTe and PdSeTe. The fourteen bands around the Fermi energy (E_{F0}), at 0 eV (blue dashed horizontal line), are in excellent agreement with the QE results.

μ^* is the effective Coulomb repulsion constant [74,75] and ω_{log} is an average phonon frequency determined by:

$$\omega_{log} = exp\left[\frac{2}{\lambda}\int\frac{\alpha^2 F(\omega)}{\omega}log\omega d\omega\right].$$ (5)

For almost all structures, $0.1 \leq \mu^* \leq 0.2$; thus the reported values of T_c will correspond to this range.

3. Convergence of the el–ph calculations

The 1T Janus structures pertain to the hexagonal geometry and spacegroup P3m1 [76] and are shown in Fig. 1. Without considering the SOC, these structures are narrow gap semiconductors with a 0.33 eV bandgap for PdSTe and 0.34 eV for PdSeTe. The equilibrium lattice vectors are found to be 3.71 and 3.81 Å in PdSTe and PdSeTe respectively, which are in good agreement with other theoretical predictions using the same pseudopotential [77]. Additional information including formation energies and bond lengths are already established in our previous publication [26].

Before determining λ and T_c, two convergence criteria on the initial calculations, must be verified. Firstly, the electronic band structure and the phonon dispersion curves obtained via MLWFs must be in
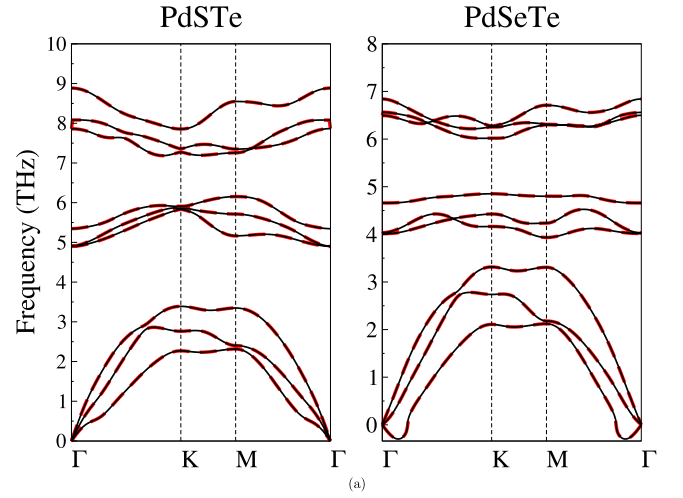
Fig. 3. (Color online). Phonon dispersion of the Janus 1T PdSTe and PdSeTe structures obtained from QE (black solid curves) and from using MLWFs (dashed red curves). Results show that the chosen MLWFs correctly reproduce the phonon dispersions of the systems.

agreement with those produced within DFT in QE. We find that the MLWF bands are best constructed using the d orbitals of the Pd species and the p orbitals of the S, Se and Te species. The electronic band structures are plotted in Fig. 2 for PdSTe and PdSeTe respectively. It can be clearly observed that the electronic bands around the Fermi level (situated at the 0 eV level) are successfully reproduced.

Fig. 3 shows the phonon dispersion curves attained through DFT using QE (dashed black curves) and those obtained by the MLWFs (red curves) for the Janus PdSTe and PdSeTe structures. Again, the agreement between the two curves is strikingly good. These graphs are equivalent to those determined using PHONOPY code [78] in [26]. Despite the dynamical stability of the structures, some small negative (imaginary) frequencies appear in the region around the point Γ [26], possibly due to numerical noise.

The second criterion for convergence is the accuracy of the Wannier interpolation technique, which is the basis of a correct calculation of the electron–phonon coupling λ. To do so, we look at the spatial localizations of the electronic Hamiltonian H^{el} and the dynamical matrix D^{ph}. The corresponding matrix elements, in the MLWFs' representation, are defined as [79]:

$$H^{el}_{\vec{R}_e,\vec{R}'_e} = \sum_{\vec{k}} w_{\vec{k}}e^{-i\vec{k}.(\vec{R}_e-\vec{R}'_e)}U^{\dagger}_{\vec{k}}H^{el}_{\vec{k}}U_{\vec{k}}$$ (6)

$$D^{ph}_{\vec{R}_p,\vec{R}'_p} = \sum_{\vec{q}} w_{\vec{q}}e^{-i\vec{q}.(\vec{R}_p-\vec{R}'_p)}D^{ph}_{\vec{q}}e^{\dagger}_{\vec{q}}$$ (7)

where $\vec{R}_e$, $\vec{R}'_e$, $\vec{R}_p$ and $\vec{R}'_p$ are unit cell positions, $w_{\vec{k}}$ and $w_{\vec{q}}$ are BZ weights, $U_{\vec{k}}$ is a unitary transformation from Bloch functions to MLWFs and $e_{\vec{k}}$ are orthonormal eigenvectors of the dynamical matrix.

The Wannier–Fourier interpolation method is based on the decay properties of the Wannier functions and the phonon perturbation in real space. It is then possible to verify how each of the quantities described in Eqs. (6) and (7) decays within the aforementioned supercells. A detailed information of this technique can be found in [79].

Fig. 4 depicts the decaying of the spatial localizations of $H^{el}_{\vec{R}_e,\vec{R}'_e}$ (call it $H(R)$) and of $D^{ph}_{\vec{R}_p,\vec{R}'_p}$ (call it $D(R)$) with distance $R = R_e - R'_e$ or $R = R_p - R'_p$ for PdSTe and PdSeTe. Within a distance of 30 Å, $H(R)$ decays to 4.2×10^{-4} and 4.8×10^{-4} for PdSTe and PdSeTe respectively. On the other hand, $D(R)$ goes down to $\sim 2.67 \times 10^{-5}$ and 1.96×10^{-5} in PdSTe and PdSeTe. These low values indicate that the chosen fine grids accurately define the electronic and phonon parts.
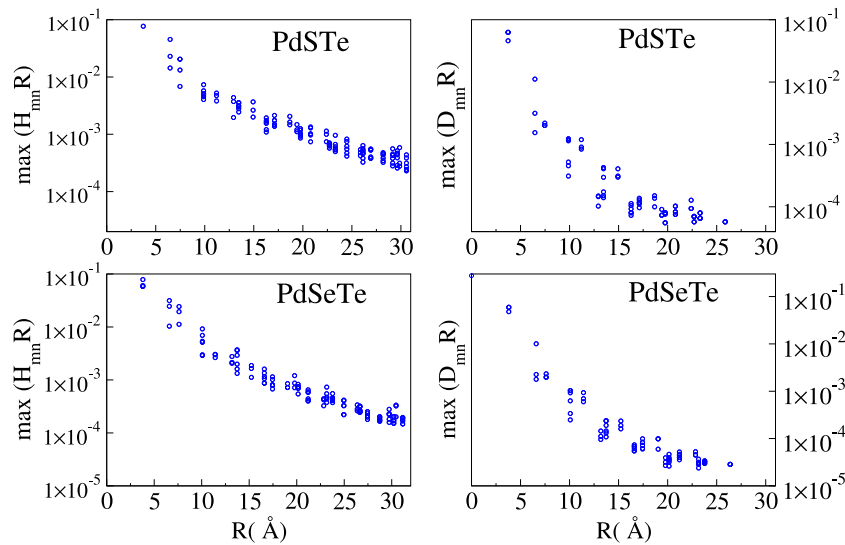
Fig. 4. Graphs on the left hand side represent the spatial decay of the electronic part of the Hamiltonian in the Wannier representation for 1T PdSTe and PdSeTe while those on the right hand side represent the spatial decay of the phonon dynamical matrices.
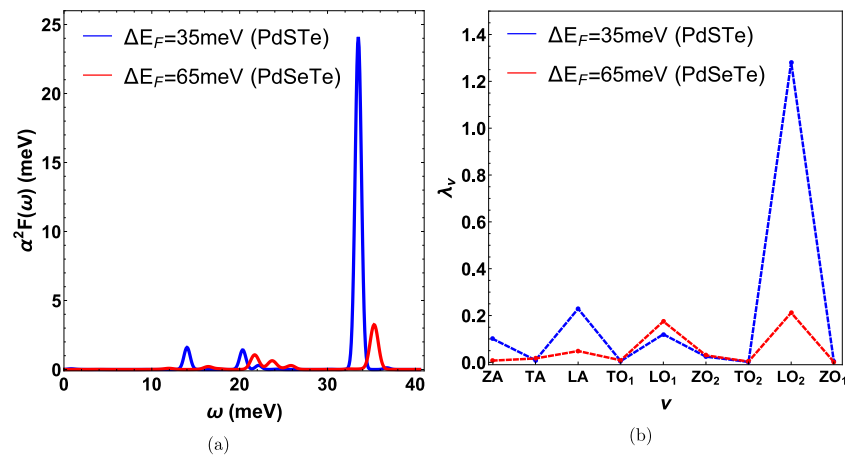
Fig. 5. (Color online) (a) Eliashberg function $\alpha^2 F(\omega)$ along the whole frequency range for 1T PdSTe and PdSeTe systems and (b) The average el–ph coupling coefficient, over the sampled fine grid of **q** points, per mode λ_ν. In both structures, the longitudinal modes give the highest contributions to the total el–ph coefficient λ. As a guide to the eye, the values have been joined by dashed lines.

4. Results and discussions

Fermi energy shifts of the form $\Delta E_F = E_F - E_{F0}$ will take on the values 35 and 65 meV for PdSTe and PdSeTe respectively, where E_F and E_{F0} refer to the shifted and unshifted Fermi energies respectively. Since E_{F0} is displaced towards the conduction bands, an increase in the number of electrons is expected. These particular values represent the minimum raise in E_{F0} needed to produce non zero values of λ in the systems considered. Based on a nearly free electron model, by supposing that the energy is quadratic near the maxima and minima of the valence and conduction bands with the mass of the electron being substituted with an effective mass, we can safely state that for a 2D system, E_F is proportional to the density of electrons per unit cell area (n). Without loss of generality, we can then mathematically write that $\Delta E_F / E_{F0} = \Delta n / n_0$, where $\Delta n = n - n_0$. Therefore knowing the electron density for the undoped system n_0, n for the various Fermi energy shifts can be consequently determined. In what follows, the doping concentration is referred to as $\Delta n / n_0 \times 100$. For PdSTe, $n_0 = 1.82 \times 10^{16}/\text{cm}^2$ and becomes $n = 1.85 \times 10^{16}/\text{cm}^2$ for $\Delta E_F = 35$ meV. In the case of PdSeTe, $n_0 = 1.75 \times 10^{16}/\text{cm}^2$ and increases to $n = 1.82 \times 10^{16}/\text{cm}^2$ for $\Delta E_F = 65$ meV. These shifts correspond to a $\sim 2\%$ doping for PdSTe and $\sim 4\%$ doping of PdSeTe. In either case, since we

can still assume that $n \approx n_0$, we can consider the Janus structures to be lightly doped. If so, the electronic and phonon dispersion bands of the undoped systems can be used to calculate λ. The nature of the dopant remains an open question that will be treated in a future publication.

Fig. 5(a) shows plots of the Eliashberg functions $\alpha^2 F(\omega)$ for PdSTe and PdSeTe versus the phonon frequencies ω, given in meV. For a 35 meV shift, we notice that PdSTe's $\alpha^2 F(\omega)$ function possesses one large sharp peak at ~ 33.57 meV, and two small peaks around 14 and 20.3 meV; this implies that high optical phonon modes contribute the most to the el–ph coupling mechanism. Similarly, for PdSeTe, the highest sharp peak appears at $\omega \sim 35.35$ meV and two smaller peaks appear in the vicinity of 21.8 and 23.8 meV.

To back up the above discussion, Fig. 5(b) displays the contribution of each of the nine vibrational modes to λ, denoted by λ_ν. These are obtained by evaluating $\sum_q \lambda_{q\nu}/N_q$, where N_q is the total number of sampled phonon **q**-points. The x-axis depicts the nine modes of vibration; "ZA", "LA", "TA" are the flexural, longitudinal and transverse acoustical modes while "ZO", "LO" and "TO" denote the flexural, longitudinal and transverse optical modes with two types for each mode, referred to as "1" and "2". In PdSTe, contributions from the longitudinal high optical modes and the longitudinal acoustic mode are manifest; for $\Delta E_F = 35$ meV, LO_2 contributes about 72% and LA
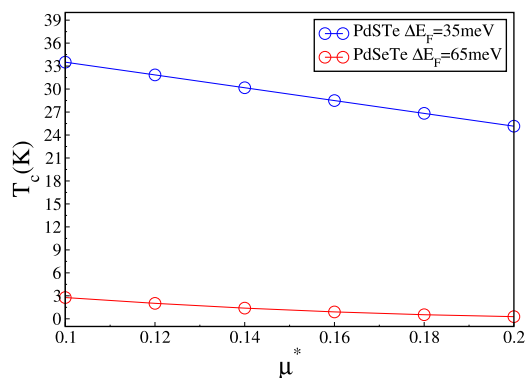
Fig. 6. (Color online) The change of the McMillan–Dynes critical temperature T_c as a function of the screened Coulomb potential μ^*. The values have been joined by continuous lines.

$\sim 32\%$ to the total λ. The role of the low lying optical mode LO_1 is revealed, in PdSeTe: for $\Delta E_F = 65$ meV, the highest contributions to the overall λ come from both LO_1 ($\sim 35\%$) and LO_2 ($\sim 42\%$). The longitudinal acoustic (LA) mode still contributes but with only $\sim 9\%$.

PdSTe reaches a cumulative $\lambda = 1.77$ for $\Delta E_F = 35$ meV, whereas PdSeTe has $\lambda = 0.50$ for a 65 meV shift. Therefore PdSTe has an advantage over PdSeTe, reaching a higher value of λ, for a smaller Fermi energy shift. Using Eq. (4), we obtain for the minimum superconducting temperature values $T_c = 28.19$ K and 0.28 K for PdSTe and in PdSeTe respectively, corresponding to $\mu^* = 0.2$. For the complete range $0.1 < \mu^* < 0.2$, $28.19 < T_c < 33.51$ K for PdSTe and $0.28 < T_c < 2.77$ K for PdSeTe. Fig. 6 shows the variation of T_c with respect to μ^* for both systems.

Two remarks are in order here: Firstly, no higher Fermi energy shifts have been considered in this study because these will correspond to higher electron doping concentrations. Albeit, this generates larger el–ph coupling parameters, these scenarios cannot be treated within RBA as they imply a heavy doping mechanism. Secondly, our choice to investigate PdSTe and PdSeTe in particular is because, again in these systems, small Fermi energy shifts induce small (the smallest) doping levels. As far as the electron–phonon coupling in other Pd TMDs, such as 1T PdS_2, $PdSe_2$ and PdSSe is concerned, our calculations demonstrate that ΔE_F takes on minimum values of around 100 meV, 300 meV and 500 meV respectively to produce a significant el–ph coupling. These values are large compared to those of PdSTe and PdSeTe and will correspond to doping levels larger than 4%. In fact, the above values are equivalent to a 5.4%, 16.2% and 23.54% doping in PdS_2, $PdSe_2$ and PdSSe respectively. Such high doping levels, principally in $PdSe_2$ and PdSSe, cannot be discussed within the framework of RBA since important changes in the electronic and phonon band structures cannot be neglected.

Comparing the T_c values of the systems in question to those for other superconducting structures in the literature, undoped β_{12} and χ_3 type borophenes are superconductors with $T_c = 18.7$ K and 24.7 K respectively [12] ($\mu^* = 0.1$ is used). For the same value for μ^*, lightly doped 1T PdSTe is expected to register higher T_c values. These superconducting temperatures are also larger than those of graphene deposited on Li (8.1 K) [80], doped silicene with 0.44e/atom (7.1 K) [81], doped phosphorene with 0.1 e/atom (4.2 K) [82], stanene deposited on Li (1.3 K) [83], doped arsenene under a biaxial tensile strength of 4% [53] and the 2D Mo_2B_2 systems with $T_c = 3.9$ K and 0.2 K for tetra and tri forms respectively.

As far as TMDs are concerned, the semi metal $PdTe_2$ was recently reported to be a type-I superconductor with $T_c \sim 1.64$ K [84]. Also bulk semi metal $MoTe_2$ is superconducting with $T_c \sim 0.1$ K which increases to 8.2 K upon the application of an 11.7 GPa pressure [85]. Proximity induced superconductivity in WTe_2 is discussed in [86], where it has

been found that a 42 nm thick layer of WTe_2 is superconducting with $T_c = 1.2$ K.

Moreover metallic 1T and 1T′ phases of MoS_2 demonstrate a superconducting behavior when intercalated with potassium K reaching $T_c = 2.8$ and 4.2 K respectively [87]. For Pd TMDs, pressure induced superconductivity in the pyrite phases of $PdSe_2$ [88] and PdS_2 [89] have been considered. These values are still smaller than the T_c determined for the lightly doped PdSTe system considered in this work.

5. Conclusion and final considerations

This work presents a preliminary study on the induction of superconductivity in the semiconducting 2D 1T Pd Janus structures PdSTe and PdSeTe, by slightly increasing their Fermi energies (electron or n doping) and verifying the enhancement in their el–ph coupling. The corresponding results are considered reasonable within the Rigid band approximation (RBA) when both the electronic and phonon band structures of the systems do not get largely affected by the shifts. These two systems should fit in the above description because the small displacements in the Fermi energy do not cause a large variation in the electronic concentration. Indeed, our results demonstrate that variations as small as 35 meV and 65 meV in PdSTe and PdSeTe respectively, produce measurable el–ph coupling coefficients, calculated to be 1.77 in PdSTe and 0.5 in PdSeTe with minimum values of the superconducting temperatures of ~ 28.19 K and 0.28 K for PdSTe and PdSeTe respectively; moreover the new electron densities remain in the order of the initial electron densities. Interestingly, longitudinal acoustic and optical vibrational modes contribute the most to the el–ph coupling in both systems.

However, the RBA should fall apart for other Pd TMDs, namely PdS_2, $PdSe_2$ and PdSSe, which require larger shifts in the Fermi energies to enhance the el–ph interactions. This corresponds to $\sim 16\%$ electron doping in $PdSe_2$ and $\sim 23\%$ in PdSSe. In these situations, the band structures of the undoped systems cannot be used to obtain the el–ph coupling coefficient and the corresponding T_c. Consequently, RBA cannot be used to predict the el–ph coupling in these systems, since the above high percentages imply that the new electron concentrations become distant from the initial concentrations, a sign of heavy doping.

The results presented in this manuscript are intended to be preliminary, investigating the minimum requirements to strengthen the el–ph coupling in Pd Janus structures. They indicate that T_c for PdSTe is largest and is larger than superconduction temperatures registered for other 2D materials already studied including borophene, stanene, phosphorene and arsenene as well as other TMDs.

To verify the validity of the RBA results presented in this manuscript, PdSTe and PdSeTe must be doped with atoms that promote n-doping and whose electron concentration percentages match the ones discussed in this work. Fermi energy shifts, electronic band structures and phonon dispersion bands can then be obtained. This allows the computation of the el–ph coupling λ and T_c, whose values can be compared against the ones estimated in this study. The electronic and phonon band structures of the lightly doped structures would also facilitate the evaluation of the superconducting gaps, in an attempt to obtain better estimates of T_c as well as the electron–phonon quasiparticle corrections to the Kohn–Sham (KS) energies.

CRediT authorship contribution statement

Elie A. Moujaes: Conception and design of study, Acquisition of data, Analysis and/or interpretation of data, Writing – original draft, Writing – review & editing, Response to the referees' comments. **W.A. Diery:** acquisition of data, Analysis and/or interpretation of data, Writing – review & editing, Response to the referees' comments.

Declaration of competing interest

The authors declare that they have no known competing financial interests or personal relationships that could have appeared to influence the work reported in this paper.

Data availability

The data that supports this study are available within this article.

Acknowledgments

References

[1] R.E. Peierls, Helv. Phys. Acta 7 (1934) 81–83.
[2] N.D. Mermin, Phys. Rev. 176 (1968) 250–254.
[3] A.K. Geim, K.S. Novoselov, Nature Mater. 6 (2007) 183.
[4] A.H. Castro Neto, F. Guinea, M.M.R. Peres, K.S. Novoselov, A.K. Geim, Rev. Modern Phys. 81 (2009) 109.
[5] H. Kawamoto, Proc. IEEE. 90 (2002) 460–500.
[6] K. Emery, C. Osterwald, Sol. Cells 21 (1987) 313–327.
[7] A.K. Geim, Science 324 (2009) 1530–15344.
[8] F. Liu, P. Ming, J. Li, Phys. Rev. B 76 (2007) 064120.
[9] J. Sone, T. Yamagami, Y. Aoki, K. Nakatsuji, Hiroyuki. Hirayama, New J. Phys. 16 (2014) 095004.
[10] M.E. Dávila, G. Le Lay, Sci. Rep. 6 (2016) 20714.
[11] A. Carvalho, M. Wang, X. Zhu, A.S. Rodin, H. Su, A.H. Castro Neto, Nat. Rev. Mater. 1 (2016) 16061.
[12] A.J. Mannix, X.-F. Zhou, B. Kiraly, J.D. Wood, D. Alducin, B.D. Myers, X. Liu, B.L. Fisher, U. Santiago, J.R. Guest, M.J. Yacaman, A. Ponce, A.R. Oganov, M.C. Hersam, N.P. Guisinger1, Science 350 (2015) 1513–1516.
[13] M. Dong, C. He, W. Zhang, J. Phys. Chem. C 121 (2017) 22040–22048.
[14] L.G.P. Martins, M.J.S. Matos, A.R. Paschoal, P.T.C. Freire, N.F. Andrade, A.L. Aguiar, J. Kong, B.R.A. Neves, A.B. de Oliveira, M.S.C. Mazzoni, A.G. Souza Filho, L.G. Cançado, Nature Commun. 8 (2017) 96.
[15] X-Long. Yu, L. Huang, J. Wu, Phys. Rev. B 95 (2017) 125113.
[16] J. Yuhara, B. He, N. Matsunami, M. Nakatake, G. Le Lay, Adv.Mater. 31 (2019) 1901017.
[17] J. Gusakova, X.L. Wang, L.L. Shiau, A. Krivosheeva, V. Shaposhnikov, V. Borisenko, V. Gusakov, B.K. Tay, Phys. Status Solidi A 214 (2017) 1700218.
[18] V. Ongun Özçelik, J.G. Azadani, C. Yang, S.J. Koester, T. Low, Phys. Rev. B 94 (2016) 035125.
[19] H.-P. Komsa, J. Kotakoski, S. Kurasch, O. Lehtinen, U. Kaiser, A.V. Krasheninnikov, Phys. Rev. Lett. 109 (2012) 035503.
[20] Yi. Ding, Y. Wang, J. Ni, L. Shi, S. Shi, W. Tang, Physics B 406 (2011) 2254–2260.
[21] R.J. Toh, Z. Sofer, M. Pumera, J. Mater. Chem. A 4 (2016) 18322–18334.
[22] H. Guo, N. Lu, L. Wang, X. Wu, X.C. Zeng, J. Phys. Chem. C 118 (2014) 7242–7249.
[23] A.-Y. Lu, H. Zhu, J. Xiao, C.-P. Chuu, Y. Han, M.-H. Chiu, C.-C. Cheng, C.-W. Yang, K.-H. Wei, Y. Yang, Y. Wang, D. Sokaras, D. Nordlund, P. Yang, D.A. Muller, M.-Y. Chou, X. Zhang, L.-J. Li, Nat. Nanotechnol. 12 (2017) 744–749.
[24] S.-D. Guy, Y.-F. Guo, X.-S. Guo, Comput. Mater. Sci. 161 (2019) 16–23.
[25] S. Deng, L. Li, O.J. Guy, Y. Zhang, Phys. Chem. Chem. Phys. 21 (2019) 18161–18169.
[26] E.A. Moujaes, W.A. Diery, J. Phys. Condens. Matter. 31 (2019) 455502.
[27] C. Buzea, T. Yamashita, Supercond. Sci. Technol. 14 (2001) R115.
[28] P. Pęczkowski, P. Szterner, Z. Jaegermann, M. Kowalik, R. Zalecki, M. Woch, J. Supercond. Nov. Magn. 31 (2018) 2719.
[29] J. Prakash, S.J. Singh, S.L. Samal, S. Patnaik, A.K. Ganguli, Europhys. Lett. 84 (2008) 57003.
[30] D. Drung, C. Assmann, J. Beyer, A. Kirste, M. Peters, F. Ruede, Th. Schurig, IEEE Trans. Appl. Supercond. 17 (2007) 699–704.
[31] A.L. Fetter, J.D. Walecka, Quantum Theory of Manyparticle Systems, McGraw-Hill Book Company, 1971.
[32] E. Snider, N. Dasenbrock-Gammon, R. McBride, M. Debessai, H. Vindana, K. Vencatasamy, K.V. Lawler, A. Salamat, R.P. Dias, Nature 586 (2020) 373–377.
[33] J. Chapman, Y. Su, C.A. Howard, D. Kundys, A.N. Grigorenko, F. Guinea, A.K. Geim, I.V. Grigorieva, R.R. Nai, Sci. Rep. 6 (2016) 23254.
[34] Y. Cao, V. Fatemi, S. Fang, K. Watanabe, T. Taniguchi, E. Kaxiras, P. Jarillo-Herrero, Nature 556 (2018) 43–50.
[35] S. Ichinokura, K. Sugawara, A. Takayama, T. Takahashi, S. Hasegawa, ACS. Nano 10 (2016) 2761–2765.
[36] A.P. Durajski, K.M. Skoczylasb, R. Szcz eśniaka, Phys. Chem. Chem. Phys. 21 (2019) 5925–5931.
[37] M. Strongin, O.F. Kammerer, J. Appl. Phys. 39 (1968) 2509–2514.
[38] J.M. Graybeal, M.R. Beasley, Phys. Rev. B 29 (1984) 4167–4169.
[39] H.M. Jaeger, D.B. Haviland, A.M. Goldman, B.G. Orr, Phys. Rev. B 34 (1986) 4920–4923.
[40] D.B. Havil, Y. Liu nad A.M. Goldman, Phys. Rev. Lett. 62 (1989) 2180–2183.
[41] Y. Liu, D.B. Haviland, B. Nease, Goldman. A.M., Phys. Rev. B 47 (1993) 5931–5946.
[42] T. Terashima, K. Shimura, Y. Bando, Phys. Rev. Lett. 67 (1991) 1362–1365.
[43] C. Dekker, P.J.M. Woltgens, Phys. Rev. Lett. 69 (1992) 2717–2720.
[44] T. Nishio, M. Ono, T. Eguchi, H. Sakata, Y. Hasegawa, Appl. Phys. Lett. 88 (2006) 113115.
[45] S. Qin, J. Kim, Q. Niu, C.K. Shih, Science 324 (2009) 1314–1317.
[46] D. Eom, S. Qin, M.Y. Chou, C.K. Shih, Phys. Rev. Lett. 96 (2006) 27005.
[47] D. Costanzo, S. Jo, H. Berger, A.F. Morpurgo, Nat. Nanotechnol. 11 (2016) 339–344.
[48] D. Malko, C. Neiss, F. Viñes, A. Görling, Phys. Rev. Lett. 108 (2012) 086804.
[49] R. Baughman, H. Eckhardt, M. Kertesz, J. Chem. Phys. 87 (1987) 6687.
[50] J. Xi, D. Wang, Y. Yi, Z. Shuai, J. Chem. Phys. 141 (2014) 034704.
[51] M. Gao, Q.-Z. Li, X.-W. Yan, J. Wang, Phys. Rev. B 95 (2017) 024505.
[52] J.-A. Yan, R. Stein, D.M. Schaefer, X.-Q. Wang, M.Y. Chou, Phys. Rev. B 88 (2013) 121403.
[53] X. Kong, M. Gao, X.-W. Yan, Z.-Y. Lu, T. Xiang, Chin. Phys. B 27 (2018) 046301.
[54] L. Yan, T. Bo, P.-F. Liu, B.-T. Wang, Y.-G. Xiao, M.-H. Tang, J. Mater. Chem. C 7 (2019) 2589–2595.
[55] S. K.Mahata, A. S.Ngankeu, N.F. Hinsche, I. Mertig, K. Guilloy, P.L. Matzen, M. Bianchi, C.E. Sanders, J.A.Miwa, H. Bana, E. Travaglia, P. Lacovig, Surf. Sci. 681 (2019) 64–69.
[56] N.F. Hinsche, K.S. Thygesen, 2D Mater. 5 (2018) 015009.
[57] E.G.C.P van Loon, M. Rösner, G. Schönhoff, M.I. Katsnelson, T.O. Wehling, Npj Quantum Mater. 3 (2018).
[58] L. Li, X. Deng, Z. Wang, Y. Liu, M. Abeykoon, E. Dooryhee, A. Tomic, Y. Huang, J.B. Warren, E.S. Bozin, S.J.L. Billinge, Y. Sun, Y. Zhu, G. Kotliar, C. Petrovic, Npj Quantum Mater. 2 (2017).
[59] R. Guo, X. Bu, S. Wang, G. Zhao, New Journal of Physics 21 (11) (2019) 113040.
[60] Y. Takagiwa, Y. Pei G. Pomrehn, G.J. Snyder, APL Mater. 1 (2013) 011101.
[61] G.H. Wannier, Phys. Rev. 52 (1937) 191–197.
[62] P. Giannozzi, S. Baroni, N. Bonini, N. Calandra, R. Car, C. Cavazzoni, et al., J. Phys. Condens. Matter. 21 (2009) 395502.
[63] N. Troullier, J.L. Martins, Phys. Rev. B 43 (1991) 1993.
[64] J. Perdew, K. Burke, M. Ernzerhof, Phys. Rev. Lett. 77 (1996) 3865.
[65] F. Giustino, M.L. Cohen, S.G. Louie, Phys. Rev. B 76 (2007) 165108.
[66] S. Poncé, E. Margine, C. Verdi, F. Giustino, Comput. Phys. Comm. 209 (2016) 116–133.
[67] A.A. Mostofi, J.R. Yates, G. Pizzi, Y.S. Lee, I. Souza, D. Vanderbilt, N. Marzari, Comput. Phys. Comm. 185 (2014) 2309.
[68] G.M. Eliashberg, Sov. Phys.—JETP 11 (1960) 696.
[69] J. Bardeen, L.N. Cooper, J.R. Schrieffer, Phys. Rev. 108 (1957) 1175.
[70] P.B. Allen, B. Mitrović, Solid State Physics, vol. 37, Academic Press, New York, 1983, pp. 1–92,
[71] J.P. Carbotte, Rev. Modern Phys. 62 (1990) 1027.
[72] P.B. Allen, Phys. Rev. B 6 (1972) 2577.
[73] P.B. Allen, R.C. Dynes, Phys. Rev. B 12 (1975) 905.
[74] C.F. Richardson, N.W. Ashcroft, Phys. Rev. Lett. 78 (1997) 118.
[75] K.-H. Lee, K.J. Chang, M.L. Cohen, Phys. Rev. B 52 (1995) 1425.
[76] C.N.R. Rao, U. Maitra, Annu. Rev. Mater. Sci. 45 (2015) 29–62.
[77] W.-L. Tao, et al., J. Appl. Phys 127 (2020) 035101.
[78] A. Togo, I. Tanaka, Phys. Rev. B 78 (2008) 134106.
[79] J. Noffsinger, F. Giustino, B.D. Malone, C.-H. Park, S. G.Louie, M.L. Cohen, Comput. Phys. Comm. 180 (2010) 2140–2148.
[80] G. Profeta, M. Calandra, F. Mauri, Nat. Phys. 8 (2012) 131–134.
[81] W. Wan, Y. Ge, F. Yang, Y. Yao, Europhys. Lett. 104 (2013) 36001.
[82] D.F. Shao, W.J. Lu, H.Y. Lv, Y.P. Sun, Europhys. Lett. 108 (2014) 67004.
[83] Y. Sahidu, O. Akin-Ojo, Comput. Mater. Sci. 118 (2016) 11–15.
[84] H. Leng, A. Ohmura, L.N. Anh, F. Ishikawa, T. Naka, Y.K. Huang, A. de Visser, J. Phys. Condens. Matter. 32 (2019) 025603.
[85] Y. Qi, P. Naumov, M. Ali, C.R. Rajamathi, W. Schenlle, O. Barkalov, M. Hanfland, Nature Commun. 7 (2016) 11038.
[86] Ce. Huang, A. Narayan, E. Zhang, Y. Liu, X. Yan, J. Wang, C. Zhang, W. Wang, T. Zhou, C. jiang, ACS Nano 12 (2018) 7185–7196.
[87] R. Zhang, I.-L. Tsai, J. Chapman, E. Khestanova, J. Water, I.V. Grigorieva, Nano Lett. 16 (2016) 629–636.
[88] M.A. ElGhazali, P.G. Naumov, H. Mirhosseini, V. Süß, L. Müchler, W. Schnelle, C. Felser, S.A. Medvedev, Phys. Rev. B 96 (2017) 060509, (R).
[89] M.A. ElGhazali, P.G. Naumov, Q. Mu, V. Süß, A.O. Baskakov, C. Felser, S.A. Medvedev, Phys. Rev. B 100 (2019) 014507.